Measurement Science and Technology, Volume 24, Number 9, 2013, Paper Number: 094001

Passive OCT probe head for 3D duct inspection

Helen D Ford and Ralph P Tatam
Department of Engineering Photonics, School of Engineering, Cranfield University, Cranfield, Bedford, MK43 0AL, UK.

E-mail: h.d.ford@cranfield.ac.uk

Abstract

A passive, endoscopic OCT probe has been demonstrated, incorporating an imaging fibre bundle and 45^{o} conical mirror, and with no electro-mechanical components at the probe tip. Circular scanning, of the beam projected onto the proximal face of the imaging bundle, produces a corresponding circular scan at the distal end of the bundle. The beam is turned through 90^{o} by the conical mirror and converted into a radially-scanned sample beam, permitting circumferential OCT scanning in quasi-cylindrical ducts. OCT images, displayed as polar plots and as 3D reconstructions, are presented, showing the internal profile of a metallic test sample containing a 65 μm step in the internal wall. Results have been acquired using two methods; one that makes use of multiple beam-circle diameters, and a mechanical "pull-back" technique. The effects of the convex surface of the conical mirror on spatial resolution are discussed, with suggested working distances given for different application regimes.

Keywords: optical coherence tomography, OCT, conical mirror, imaging fibre optic bundles, coherent fibre optic bundles, surface profiling, 3D, duct inspection.

PACS Codes: 07.6.Ly, 07.6.Vg, 42.30.Wb

1. Introduction

The potential of optical fibre imaging bundles for endoscopic OCT applications has been investigated by our group and others [1-5]. The use of imaging bundles enables an extended region of the sample to be imaged, by coupling light simultaneously [3] or sequentially [1] into multiple fibre cores within the bundle, removing the need for scanning components to be included at the probe tip. In a swept-source system of this type, imaging is achieved by coupling light in rapid succession into each element of a straight or curved row of bundle cores. Samples can be

positioned either on-axis, with the sample surface normal to the system axis, or to one side of the probe tip, with the sample surface parallel to the optical axis and a turning mirror used to rotate the beam through 90^o.

There are many situations where an OCT probe is introduced into a quasi-cylindrical structure, with the aim of acquiring images of regions on the internal wall [6, 7]. The beam in such systems is generally controlled either by miniature scanning components [8] or by a 45^o reflector that can be rotated within the probe catheter, allowing a full 360^o field of view to be accessed [7]. We propose an alternative optical delivery scheme employing an imaging bundle with conical optics in the probe tip, which obviates the need for internal moving parts within the endoscope probe. Conical mirrors have in the past been used for viewing the internal surfaces of cylindrical objects [9] and in laser speckle systems [10], and the use of such a mirror has been recently reported for OCT in combination with a piezo-electrically scanned optical fibre [11]. However, an electrically-passive OCT probe incorporating a conical mirror does not appear to have been attempted previously. There are advantages to eliminating moving components from the endoscopic section: electrical power need not now be supplied to the probe tip unless required for other processes, the potential for component failure is clearly reduced, and the mechanical arrangement is simplified. The probe tip is also likely to be more tolerant to cleaning processes in the absence of electrical components.

2. OCT system incorporating an imaging bundle and conical mirror

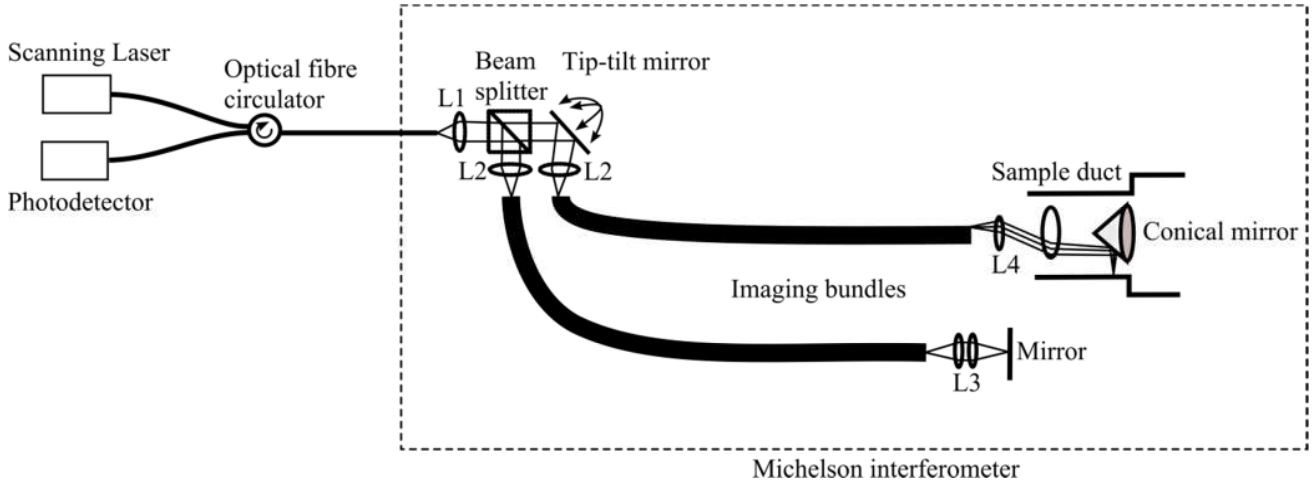

Figure 1. OCT configuration used in conical mirror experiments. L1: collimating lens, L2: focusing lenses, L3: focusing lens pair, L4: telecentric lens pair.

A 1330 nm optical coherence tomography (OCT) system, with a theoretical depth resolution, calculated from the source bandwidth, of about 8 μm in air, was constructed as described in [1], employing imaging bundles in the sample and reference arms of the interferometer (figure 1). Ideally bundle cores should be single-moded at the

operating wavelength, though in practice ours were few-moded, since standard imaging bundles commercially available are typically designed at present with visual inspection applications in mind, for which single-mode behaviour of the cores is not a priority. The number of modes supported in the near infra-red is lower than in the visible, but few-moded behaviour persists up to at least 1400 nm. Modes excited in addition to the fundamental will travel different path lengths within the bundle cores. If the difference in optical path length for two modes is within the instantaneous coherence length of the laser (about 10-20 mm for the laser used here), then interference will occur between those modes, causing the output to oscillate at frequencies dependent upon the bundle length and dispersion characteristics. The modes excited in any particular core are affected by the coupling conditions. A low NA coupling lens, an incident beam well aligned normal to the bundle input face, and centring of the beam focus within the selected core, will result in near-single-mode behaviour. However, it is not possible to ensure that these conditions apply at all times when scanning the input beam across the bundle face to access cores rapidly and sequentially.

An approximate modal analysis was performed [1], to estimate the propagation constants for the two lowest-order modes of the bundle cores at the 1330 nm centre wavelength. Exact figures for the refractive index of core and cladding were not known, but the measured output NA, and the confinement of optical power to a few low-order modes, are consistent with a V value of about 4. With these assumptions, the group delay difference between the two lowest-order modes suggests a path length difference of about 8mm for the 1350 mm long bundle. This is within the 10-20 mm coherence length of the swept source and confirms that interference effects between different modes are to be expected.

When light is coupled into a single fibre core of the bundle, a small amount of power emerges from one or more of the neighbouring cores, with a maximum of about 1.5% of the total output power appearing in any one of the six nearest neighbours [1]. In practice, the oscillations caused by intermodal and cross-coupling effects dominate other noise sources in the system. The rms magnitude of the spurious oscillations is roughly equivalent to a sample reflection of about 0.01%, which is high enough to obscure interferometric signals from typical biological tissue samples, but does allow measurements to be performed in engineering test samples. If multi-moding occurs, there is no straightforward way to eliminate the deleterious effects in this system, hence the SNR limitation. The bundle employed in the study is not optimised for this application, but was used to demonstrate the principle. It is envisaged that the method could be developed using a delivery bundle customised to ensure single-mode wave-guiding characteristics, by the use of smaller diameter cores and/or more appropriate core/cladding refractive indices.

A second bundle in the reference arm was used to ensure dispersion matching, although only one fibre core is actually required in this path. Both bundles were 1.35 m in length. A tip-tilt mirror mounted on piezoelectric actuators (PI S-334), with two-axis control, was used to control coupling of the probe beam into the sample bundle. This mirror tilts about a central pivot point in two orthogonal directions, with a maximum tilt angle of +/- 1.5^{o}. Both axes of the mirror were provided with sinusoidal drive signals of equal frequency and magnitude; application of a

90° phase shift between the two signals causes the normal to the mirror to describe a conical path in space at the specified drive frequency. Thus a beam reflected from the mirror, and passing through a focusing lens, coupled light sequentially into a circle of fibre cores, the diameter of which was proportional to the applied voltage signal.

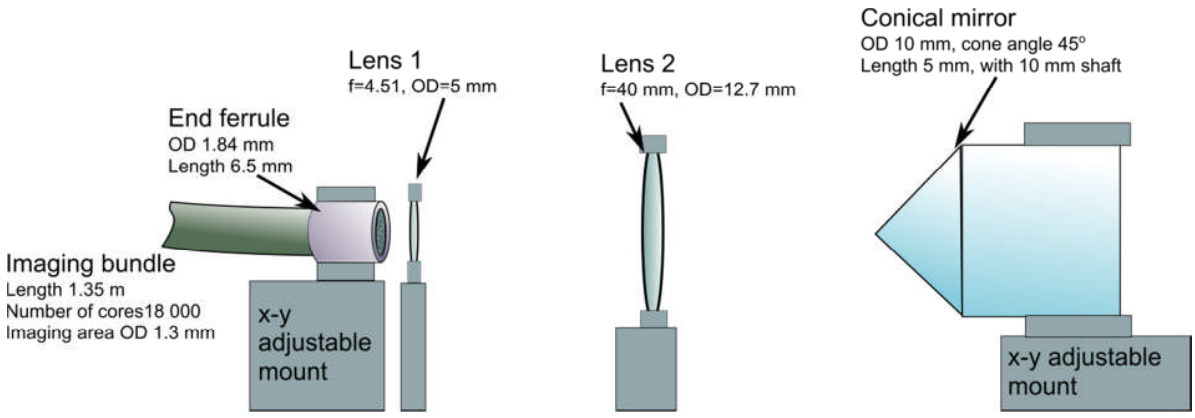

(a)

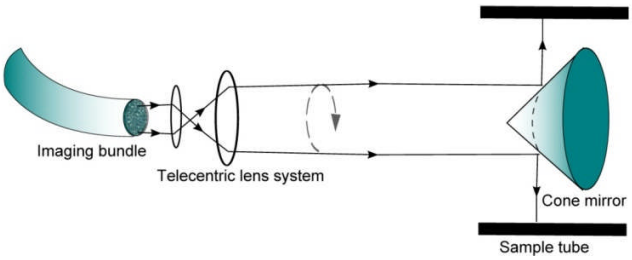

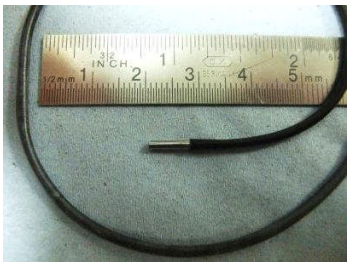

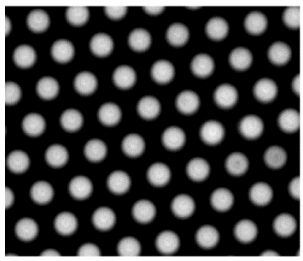

(b) **(c)** **(d)**

Figure 2. (a) Experimental set-up at probe end of bundle. (b) Simplified view showing beam paths to sample via cone mirror. (c) Photograph of bundle end ferrule, with steel rule for scale. (d) Photograph of bundle end with light coupled into cores, showing hexagonal close-packed arrangement. Image represents an area 80 μm x 64 μm.

At the probe tip, a telecentric lens pair was used to expand the output circle from the bundle from a diameter of a few hundred microns to a larger collimated circle, a few millimetres in diameter, as shown in figure 2(a,b). Photographic images of 2(c) the side view of a bundle ferrule, with a steel rule for scale, and 2(d) the end view of an illuminated bundle under high magnification, showing the packing arrangement, are also presented.

Values of the beam circle diameter, at the bundle output, were chosen to be slightly below the 10 mm base diameter of a mirrored 45° cone, 10 mm in diameter, positioned coaxially with the bundle centre and with the tip facing towards the bundle, as shown in the figure. For this cone half-angle, the probe beam is turned through 90°. Thus, if

the probe is introduced coaxially into a cylindrical duct, the beam falls radially upon the internal duct wall, describing a full circumference at the rotation frequency.

The distance between the second telecentric optic and the conical mirror was set so that beam was brought to a focus within a few hundred microns of the measurement surface. If the cone diameter greatly exceeds the beam diameter at the point of reflection, the small mirrored region responsible for the reflection can be assumed to approximate to a plane surface. The validity of this assumption is examined more closely in section 4 below.

Light is scattered from the wall of the sample and returns, via the cone and the bundle core, to the original delivery fibre, where it combines with light returning from the reference arm of the interferometer. An optical circulator was used to route the power to a detector with a 3dB low-pass cut-off at 15 MHz. Since sampling was performed at 33 MSs^{-1}, OCT frequencies above 16.5 MHz were suppressed to prevent aliasing. Conversion to a 14-bit digital signal was performed by an NI 5122 digitizer card. The scanning laser was a 1330 nm Santec HSL-2000, with a sweep rate of 20 kHz. Each A-scan, acquired during the 0.05 ms sweep period, contained 800 points after resampling into frequency space, and the mirror scan frequency was set to 33.5 Hz, allowing 600 A-scans to be acquired during each rotation of the beam around the cone mirror. The theoretical depth resolution of the system was about 8 μm. Labview™ was used both for system control and to generate and display OCT images. Hardware triggering between the mirror servo and the digitizer was implemented, to avoid the variable delay sometimes experienced between the trigger signal and onset of acquisition when software triggering is used.

Because the sample geometry for this system is quasi-circular, images are displayed as polar plots. However, some caution must be exercised in the interpretation of these: radial distance from the origin is representative not of absolute distance from the cone axis, but of the *difference* between optical path length in the sample arm and optical path length in the reference arm. The maximum accessible depth range for this system, represented by the half-width of the images, is about 2.5 mm, and is determined by the number of samples acquired within each laser sweep, via the Nyquist criterion.

Because the optical path-length varies slightly from fibre to fibre within the imaging bundle, individual A-scans experience optical path-length offsets up to a maximum of about 200 μm, causing distortions within the images, and it is necessary to apply a correction [1]. This is achieved during setup of the probe optics, with the conical mirror absent. The probe is positioned such that the output beam from the telecentric optics is focused upon a mirrored optical flat placed perpendicular to the optical axis, and an image is acquired as the beam scans the chosen circular path. The measured position of the mirror surface for each ‘A-scan’ (a point measurement, resulting in a one-dimensional intensity profile as a function of sampling depth) in the image is stored and the resulting file is subsequently used, immediately following image acquisition, to offset depth values for all sample data using that same beam circle diameter. Such corrections have been applied to all the data sets presented in this paper.

This procedure is incorporated as a straightforward step in the processing software. Calibration does not need to be repeated at each image acquisition, as the correction is constant for a particular delivery fibre. If the mechanical stability of the optics at the input end of the probe is sufficient, the required correction sets need be performed and stored once only, during probe manufacture. Moreover, in the pull-back mode described below, a single ring of fibre cores is used for all measurements and only one correction set is required. If small beam drifts do occur over time, periodic re-calibration might be desirable. This could be achieved using a calibration ring of excellent circularity, slotted over the probe tip, or by temporary removal of the conical mirror and insertion of an optical flat close to beam focus.

Let us imagine a sample piece consisting of a perfectly cylindrical duct. During one complete cycle of the tip-tilt mirror, the intersection of the scanning probe beam with the sample wall will be a circle. In aligning the measurement system, it is important to ensure coincidence of the cone axis with that of the circle swept out by the incident scanning beam. Any lateral offset between the two will result in a tilting of the measurement plane normal away from the duct axis, resulting in sampling of an elliptical region of the duct wall, rather than the expected circle. The tilt angle of the sampling plane is $2d / D$, where d is the lateral offset between cone and beam circle centres, and D is the duct diameter. To maintain tilting of the scan plane below 2^{o}, any relative axial offset must be below about 2% of the sample duct diameter. A relative tilt between the two axes will also result in an elliptical section of the duct being sampled, the tilt angle of the sampling plane being twice that of the relative mechanical misalignment. Ellipticity resulting from a lateral offset of the cone causes an axial location error, but not a depth error, whereas a tilt of the cone, relative to the beam scan axis, causes both. If looking for defects such as cracks or corrosion, the small systematic errors arising from any beam scan ellipticity are usually negligible. A problem could arise for cone tilt combined with a strongly angle-dependent reflection at polished surfaces, if the ellipticity becomes sufficiently large that most scattered light falls outside the collection NA.

Additionally, ellipticity of the sample plane arises when the optical probe axis and sample duct axis do not coincide, with effects as described above. Small angular errors between the scan plane normal and the sample axis are common to all endoscopic OCT systems, and are not peculiar to the instrument proposed here. To help maintain the probe close to the sample axis, a balloon catheter or sprung cage arrangement can be used. For critical applications, calibration against precision test objects with a known internal profile can be used to assess, and correct for, any tilt misalignment. The angular offset will be negligible for a contact probe, because the sample self-aligns parallel to the probe axis.

The transmissive region of the leached imaging bundle (Schott N.A.) was 1.3 mm in diameter, containing fibre cores in a hexagonally-packed arrangement with a centre spacing of 10.6 μm [1]. Light from the source output fibre was amplitude-divided using a beam-splitter cube. In the sample arm, the beam was turned through 90^{o}, using the tip-tilt mirror mounted at 45^{o} to the incident beam, and coupling to the bundle was achieved via an f=18.4 mm aspheric

lens. The beam waist radius at the bundle surface was about 3.5 μm. At the output of the bundle, the lens pair comprised a 5 mm diameter aspheric lens with a focal length of 4.51 mm, and a 12.7 mm diameter plano-convex lens with a focal length of 40 mm. The lens separation was equal to the sum of the focal lengths, resulting in a telecentric arrangement with a magnification of M=8.9.

The distance from the centre of the tip-tilt mirror to the input coupling lens was set approximately equal to the lens focal length of 18.4 mm, ensuring that the chief ray impinged almost perpendicularly upon the front face of the bundle, and thereby maximising coupled power. The angular tilt range of the mirror is +/- 1.5^{o}. For a given mechanical tilt, we expect an optical angular shift that is double the mechanical tilt angle. For the small angles involved, the lateral beam offset at the front face of the bundle is proportional to mirror tilt angle, having a maximum value of +/- 475 μm in the system of figure 1. With a magnification of M=8.9 for the telecentric optics, the maximum diameter of the magnified beam circle is, at 8.45 mm, slightly less than the cone base diameter of 10 mm

3. Measurements and results

For the experiments described below, the components for the probe tip were configured on an optical table, using standard optical mounts, as a proof-of-concept arrangement (figure 2(a)). To test the system, a brass ring with an internal step in the diameter, as shown in figure 3(a), was employed as a test object. The internal diameter of the ring was measured, using Vernier callipers, to be 19.06 (±0.01) mm on one side of the step, and 17.75 (±0.01) mm on the other side. Thus the depth of the step was 0.66 (±0.02) mm.

Two alternative methods can be used to obtain images from different longitudinal distances within the duct. In the first method, the amplitude of the signals applied to the tip-tilt mirror is gradually increased stepwise, resulting in beam circles of increasing diameter that intersect the conical mirror at different longitudinal positions, and therefore address different longitudinal positions within the sample. Alternatively, a beam circle of fixed diameter is defined by applying sinusoidal signals of fixed amplitude to both axes of the tip-tilt mirror. In this case, different longitudinal positions on the sample are accessed by moving the probe tip longitudinally relative to the sampled object. For single-fibre OCT probes, this is sometimes called the ‘pull-back’ method. Both techniques are demonstrated here. In these experiments, the axial translation for the second method was achieved by mounting the probe end on a high-precision translation stage. The lateral resolution of measurements made at this sample diameter is about 220 μm around the sample circumference, controlled by geometrical considerations. Best-focus considerations limit the longitudinal resolution to a value closer to 100 μm.

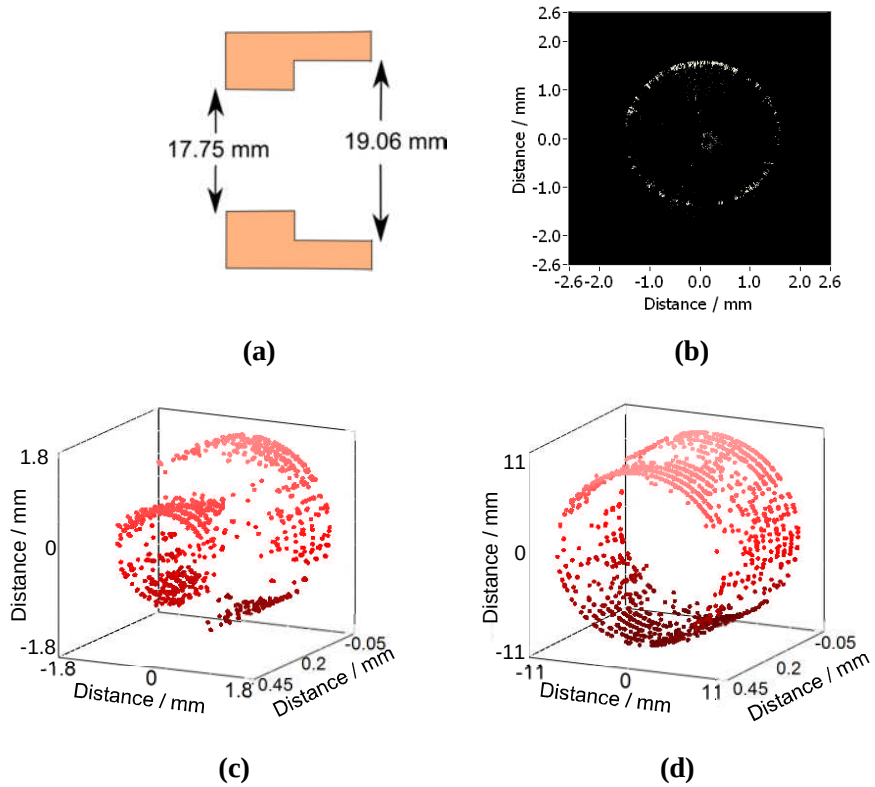

Figure 3. (a) Schematic of brass tube sample with internal step of height 0.66 mm. (b) Representative image, from the first data file in the set. (c) 3D representation of the internal tube profile created from 11 stacked images, at 42 μm intervals, using a different beam circle diameter for each image. (d) 3D representation as before, with a constant added to all depth values to obtain a tube profile corresponding to absolute physical distances.

Multiple beam-circle method

The amplitude of the signals applied to the tip-tilt mirror was increased step-wise, causing the beam-circle diameter at the bundle input to expand incrementally, in steps of 9.4 μm. The corresponding beam-circle diameter at the cone increased from 6.68 mm to 7.52 mm in steps of 84 μm, resulting in a set of 11 images separated by a longitudinal distance interval of 42 μm. A representative OCT image is shown in figure 3(b), and a 3D image, obtained by locating the maximum of the OCT image at each radial position, then stacking data for the full set of 11 images, is shown in figure 3(c). Signal intensity varies with position, due to variations in finish and cleanliness of the internal surface of the sample, therefore thresholding has been used to eliminate false maxima for radial positions where the SNR is insufficient. The step in the internal profile of the sample can readily be seen in the 3D image. As discussed above, the original OCT images show relative distance only, within a depth range of 2.5 mm; in a second 3D representation, shown in figure 3(d), a constant has been added to the depth values such that the radial distances, measured from the origin, now correspond to actual physical values for the sample tube used. This has been done

purely for illustrative purposes, to emphasise the small depth of the step in comparison with the overall average tube diameter. The radius value was obtained using Vernier callipers. In a real measurement situation, the value of the duct radius would not always be available, nor in fact required, because it is usually the magnitude of small surface defects, or variations in surface profile, that are of interest in such measurements, rather than the absolute distance from the axis of the duct.

The multiple beam-circle method allows only a limited longitudinal range within the sample duct to be accessed. In principle, this range is equal to the base-tip height of the conical mirror. However, at sites closer to the tip of the cone, excessive beam-spreading occurs, in the plane of the beam circle, caused by the diminishing radius of curvature of the mirrored surface. In practice, the axial range for this sample, using the 5 mm high conical mirror is limited to about 2.5 mm. A further disadvantage of the method is that the lateral resolution depends on beam circle diameter, via the number of fibre cores present around the circumference of a circle of given diameter, and therefore differs for images acquired at different longitudinal positions.

Pull-back method

In this 3D imaging method, a fixed signal amplitude was applied to each axis of the mirror, corresponding to a beam circle diameter of 7.01 mm. The instrument probe tip was displaced longitudinally, relative to the sample, using a translation stage, the step interval being 62.5 μm, or 1/8 of the full-circle micrometer screw rotation. This technique overcomes the range limitations of the multiple beam-circle method, allowing data to be acquired over greater longitudinal distances and with constant lateral resolution at all longitudinal positions. A set of 40 images was acquired over a distance of 2.5 mm to demonstrate the technique. Representative images from the set are shown in figure 4(a-d). A 3D plot was generated as above, by identification of the maxima at each radial position, followed by stacking data from all images, and is shown in figure 4(e). In figure 4(f), a constant corresponding to the actual radius of the duct was added to each depth value, as in figure 3(c), to generate a 3D image more representative of the actual sample piece dimensions.

Once again, the measured diameter decreases, as expected, as the scanning beam circle crosses the internal step in tube diameter. In these measurements, the probe was deliberately arranged to lie at a slight angle to the centre axis of the sample tube. The beam-scan circle therefore encounters the step in the sample diameter on one side of the tube earlier on one side of the tube than on the side diametrically opposite, leading to the form of the images seen in figure 4(a-d). It is similarly clear from the 3D representations in figures 4(e,f) that the step appears to fall at a slant across the sample, relative to the axes of the beam-scan circles.

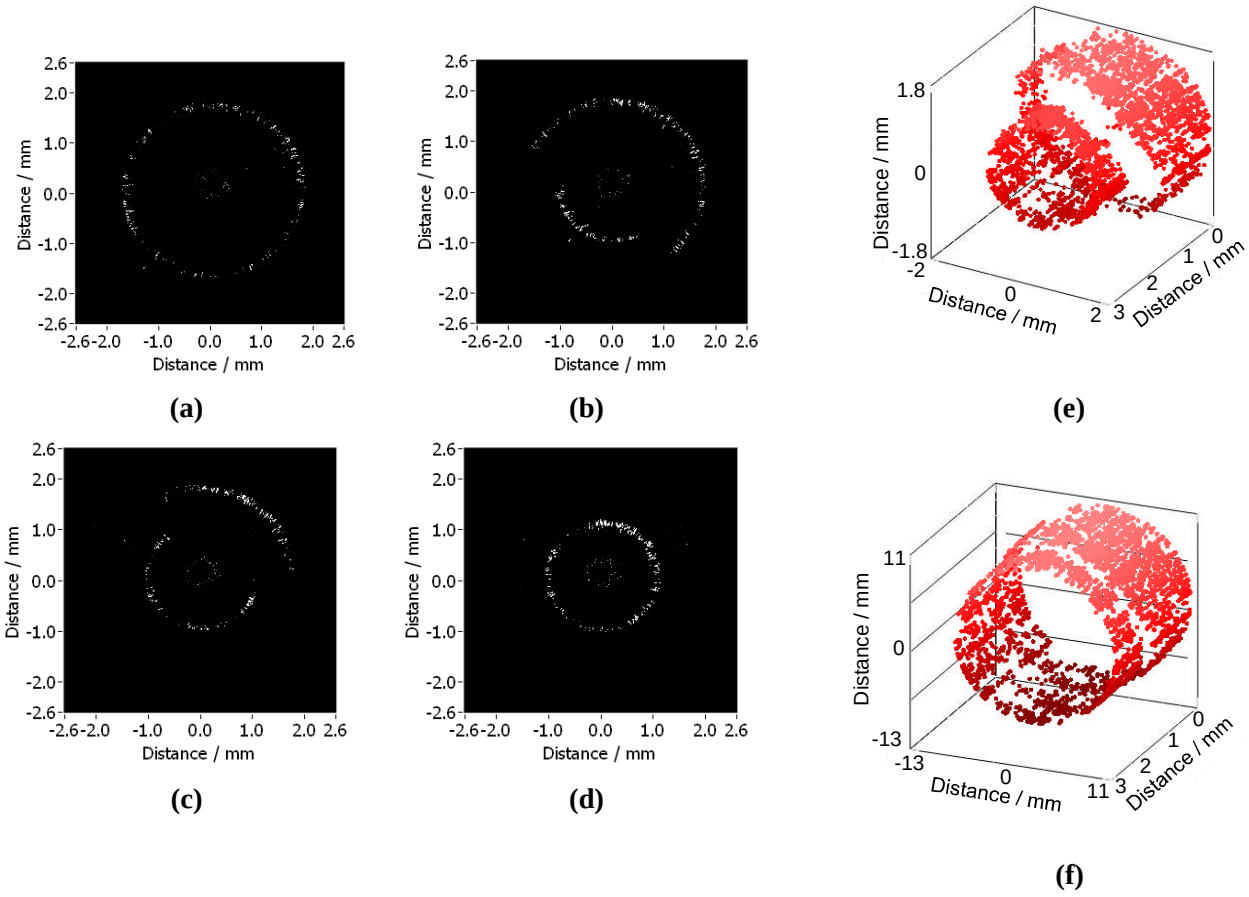

Figure 4. (a-d) Representative images at axial distances in the tube of 0.25 mm, 0.875 mm, 1.5 mm and 2.125 mm respectively. (e) 3D representation of the internal tube profile created by stacking 40 images, at 62.5 μm intervals, using longitudinal displacement of the probe tip. (f) 3D representation as in (e), with a constant added to all depth values to obtain a tube profile corresponding to absolute physical distances.

The features of the multiple beam circle and pull-back techniques are summarised in table 1, allowing a rapid side-by-side comparison of the two methods.

Table 1. Comparison of multiple beam circle and pull-back imaging methods.

	Multiple beam circle method	**Pull-back method**
Maximum longitudinal range	Approx. half of conical mirror length. *1 mm for 2 mm cone radius* *2.5 mm for 5 mm cone radius* *10 mm for 20 mm cone radius*	Limited only by range of component used to translate probe. *10-100 mm typical*
Number of sampling points in scan	Dependent on fibre core spacing. *220 μm circle radius in bundle: ~140* *450 μm circle radius in bundle: ~280*	Can be set to a high, fixed value. *390 μm circle radius in bundle: ~250*
Datasets required for depth correction	Equal to number of images required at each measurement site.	One
Minimum longitudinal resolution	Dependent on fibre core spacing. *~10.6 μm, or focused beam waist diameter if larger*	Typically dominated by beam waist diameter, as translation component can have few-micron resolution.
Minimum radius of sample duct	Cone radius, plus the thickness of probe window, if any.	
Maximum radius of sample duct (beam waist diameter 2 x best focus in absence of cone). No longitudinal adjustment of conical mirror.	Approx. 1.5 x maximum usable radius of cone mirror *2.5 mm for 2 mm cone radius* *7 mm for 5 mm cone radius* *30 mm for 20 mm cone radius*	
Maximum radius of sample duct (beam waist diameter 4 x best focus in absence of cone). Longitudinal adjustment of conical mirror to optimise.	Approx. 4 x maximum usable radius of cone mirror *6 mm for 2 mm cone radius* *18 mm for 5 mm cone radius* *80 mm for 20 mm cone radius*	

4. Discussion

Although an imaging bundle has been employed for beam transmission, access to the full surface area of the bundle is not generally necessary to make the type of measurement described in this paper. An annular region of the bundle, a few hundred microns in width, is actually used in the first imaging method and, in the second method, the beam circle diameter is fixed so that only fibre cores intersecting this ring, a few microns in width, are actually required.

In the multiple beam-circle method, a different path-length correction file is required for each set of fibre cores corresponding to one particular circle diameter. Therefore, correction data were stored for each separate voltage setting and corresponding ring of fibres. If any movement occurs at a later stage between the input optics and the bundle, new sets of correction data must be stored. The technique in which the probe is drawn backwards along the

measurement duct, ideally at a constant rate, while using a fixed ring of fibres within the bundle to generate the beam circle, is known as the 'pull-back' technique [12]. This is a preferable technique in many situations, for reasons already outlined above. Additionally, correcting for differences in the optical path length between fibre cores at different sites is eased by using only a single ring of cores, since the same set of stored correction data can now be employed for all images.

In the experiments described here, the experimentally-determined depth resolution is not as high as predicted from the source bandwidth, because the multimode behaviour of the bundle causes unwanted fluctuations in the intensity at the detector that broaden, and degrade the quality of, the coherence function such that it is no longer a smooth Gaussian. The effect of this can be seen in figure 5, for four image regions, each corresponding to the signal from a single, smooth surface. The width (FWHM) was calculated for 16 plots, yielding an average value for the depth resolution of 34 (± 15) μm. This reduced depth resolution, however, is an artefact of the multi-mode bundle behaviour, and is not fundamental to the conical mirror geometry.

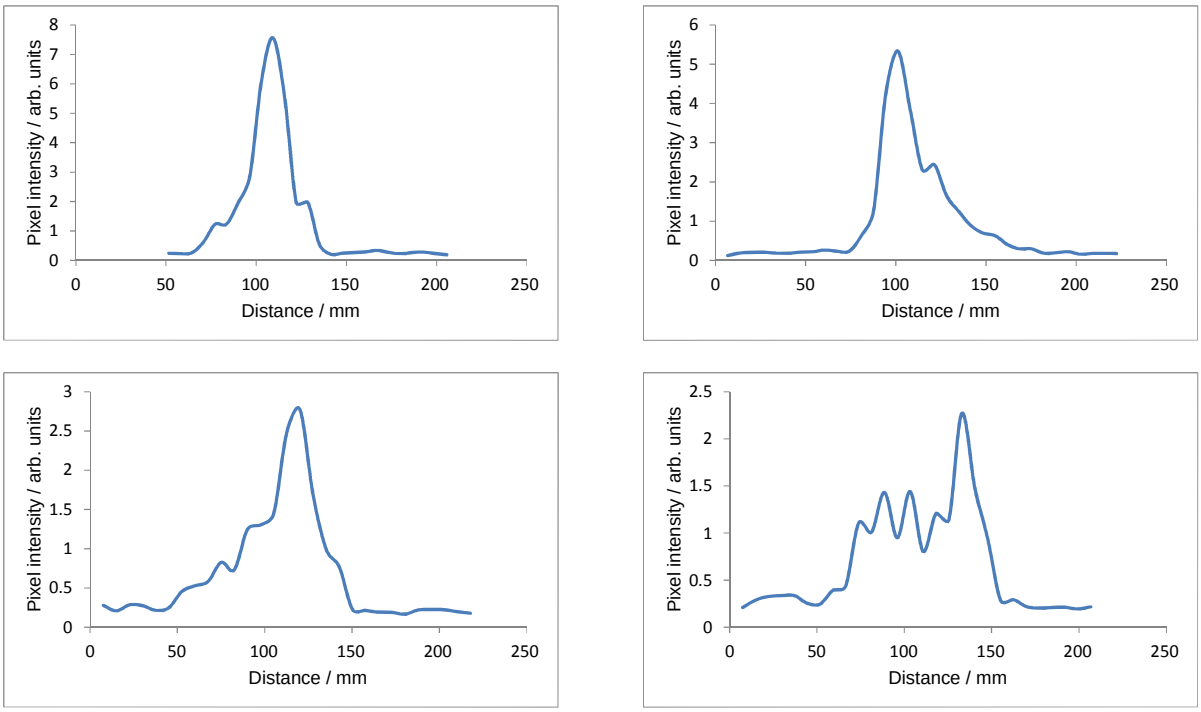

Figure 5. Smoothed plots of pixel intensities at four image positions, each representing the OCT signal for a single, smooth surface, showing the effect of multi-mode behaviour on FWHM peak widths. The plots show widths ranging from from 13 μm to 59 μm. The mean from 16 image points was measured to be 34 (± 15) μm.

Specular reflection at the measurement surface will result in loss of signal for duct cross-sections deviating significantly from a circle, because beams will "walk off" from the duct wall, and returning light will not be re-

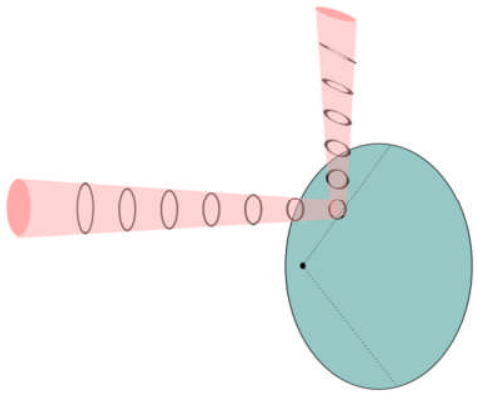

Figure 6. Effect of astigmatism, introduced by conical mirror curvature, on beam focus at a distance from the cone surface.

coupled into the bundle. Scattering tissue from a sample such as the surface of a blood vessel or gastro-intestinal tube is a more typical target for OCT investigation. Deviation from circularity is less problematic in imaging this type of sample, as light incident upon the surface is scattered in all directions. The level of scattered signal power, however, is much lower for turbid tissue samples. At present, most commercially-available imaging bundles suffer high losses in the NIR wavelength range, and those that we have been able to obtain are also few-moded in the visible and NIR. Unfortunately, the non-singlemode behaviour, and small levels of cross-talk between fibre cores, leads to interferometric artefacts [1] which are of a magnitude comparable to the OCT signals, preventing satisfactory images being obtained from biological samples with currently available imaging bundles. However these difficulties are not fundamentally limiting, and could be alleviated by different designs of fibre bundle, more appropriately designed for use with coherent imaging systems.

We have supposed above that the beam waist at the surface of the conical mirror is sufficiently small that we can treat the relevant reflecting region as a plane surface. In many situations, mirrored cones with base diameters of only a few millimetres are likely to be of interest in OCT measurements, and this approximation will not be true. For a beam of a particular numerical aperture (NA), incident on the cone surface, the NA of the reflected beam will always be unchanged in a plane parallel to the axis of the cone. Let us assume a system in which the beam reflected from the cone is brought to focus, in a plane parallel to the cone axis, on a sample. The NA will, however, be reduced or possibly even reversed in sign, because of the surface convexity in the orthogonal plane, parallel to the local circumference of the cone, as shown in figure 6.

Assuming small angles, if the sample surface is distant from the cone surface by about half of the local value of the radius, the NA, and therefore the measurement resolution, in this plane will be reduced, via a doubling of the Gaussian beam waist radius at focus. As the sample surface becomes more distant from the cone surface, the decrease in NA accelerates, and as this distance approaches the local value of the cone radius, the beam becomes

almost collimated in the circumferential plane, and spatial resolution decreases by one to two orders of magnitude compared with that of the same beam reflected from a plane surface. Small readjustments of the longitudinal position of the cone can slow the deterioration in resolution at still larger sample distances, by selecting a compromise focus between the axial and circumferential planes.

Spatial resolution also reduces linearly with radial sample distance because the number of sampling points in the circular scan is fixed, being a function of the number of fibre cores intersecting the beam circle. If the diameter of the conical mirror is several times larger than that of the imaging bundle, the resolution is determined by this geometrical limitation, for short working distances from the cone. As the working distance increases, astigmatic defocus becomes increasingly important and may start to dominate. However, astigmatic defocus can be partially controlled by adjusting the longitudinal cone position relative to the lenses, as described above. Taking this into account, the geometric effect will once again be more important at distances several times larger than the local cone radius. Note that an increased beam waist at focus also implies that scattered signal power levels will be significantly reduced at larger sample distances.

We conclude that a system for high spatial-resolution OCT imaging would require a relatively large bundle, perhaps 3-4 mm in diameter, and a cone of similar diameter. Sample distances will need to be maintained within about half the radius of the cone at the point of beam incidence, implying a contact probe in most situations. However, for measurements on inorganic ducts such as the test object used in this paper, where the application might be defect or damage detection, spatial resolutions in the 10-20 μm range are not always necessary, and surfaces are often more strongly scattering, partially compensating for the drop in signal power at larger working distances. Spatial resolution values of a few tens to a few hundreds of micrometres will often be acceptable, implying that longer working distances can be used. Although the convexity of the cone surface imposes particularly stringent requirements on working distance, similar considerations also apply in other, small diameter, OCT probes, since high-resolution imaging always depends on maintaining a sufficient value of NA at the sample surface. A general rule, for good performance with cones of dimensions less than 1 cm, is to match the cone base diameter as closely as possible to the minimum diameter expected in the intended samples.

It is worthwhile to comment briefly on the alignment issues involved in manufacturing an engineered version of such a device. A full analysis is outside the scope of this paper, but we consider here the manufacturing tolerances on the lenses and conical mirror to be aligned in the probe head. Lens de-centration (the offset between the physical and optical axes of the component) is typically about 50 μm, but can be down to 20 μm in precision components. A relative offset of 50 μm between the two lenses will result in a beam-circle tilt of less than 5 arcmin, which can be neglected. The diameter tolerance on the conical mirror is +0/-50 μm and the angular tolerance ±6 arcmin. Machining tolerances for the surrounding mounts are of similar magnitude. A small lateral offset of the bundle can be compensated by slightly altering the centre position of the selected circle of fibre cores used to generate the beam

scan. Some z- adjustment on the conical mirror would be required during manufacture, to ensure optimal focusing, and could be advantageous as a user adjustment. However, using self-centring optical mounts, x-y adjusters should be unnecessary, thus retaining the advantage of minimal probe-head complexity.

We assume that ducts inspected using such a system are likely to be quasi-cylindrical, although there will be some variation of radius as a function of beam angle. To minimise both optical power losses and variations in optical path-length to the sample surface, it is desirable for the measurement probe to be positioned close to the centroid of the duct. This could be achieved by the use of a balloon catheter surrounding the probe (particularly suitable for biological measurements) or by mounting the probe in a sprung cage arrangement appropriate to the material and surface finish of the duct under investigation. A contact probe, for high-resolution inspection of sub-surface wall structure in flexible tubes, would require the probe diameter to be closely similar to that of envisaged samples, such that the probe is automatically centred in the duct and allows for a very short working distance relative to the cone dimensions.

5. Conclusions

In conclusion, it has been demonstrated that an imaging fibre bundle, in combination with a conical mirror, can replace mechanical scanning components in the endoscopic section of a remote-viewing OCT system, allowing construction of a passive probe with circumferential scanning capability. The optical arrangement at the probe tip requires only two miniature lenses and the conical mirror, with electromechanical scanning removed to the input end of the bundle. A system appropriate for surface-profiling and defect-detection applications on engineering test samples has been demonstrated achieving, as outlined above, a depth resolution of 8 μm and lateral resolutions of about 220 μm and 100 μm, in planes parallel and perpendicular respectively, to the axis of the cone, for an object of internal diameter about 18 mm.

Acknowledgments

This work was supported by grants EP/F034679/1 and EP/H02252X/1 from the UK Engineering and Physical Sciences Research Council (EPSRC).

References

[1] Ford H D and Tatam R P 2011 Characterisation of optical fibre imaging bundles for swept-source OCT *Appl. Opt.* **50** 5 627-40

[2] Ford H D and Tatam R P 2005 Full-field optical coherence tomography *SPIE Optical Metrology Symposium (micro- and nano-technology conference), Proc. SPIE 5858 (Munich, Germany, 13-17 June 2005)* 58580J

[3] Ford H D and Tatam R P 2007 Fibre imaging bundles for full-field optical coherence tomography *Meas. Sci. Technol.* **18** 9 2949-57

[4] Xie T, Mukai D, Guo S, Brenner M and Chen Z 2005 Fiber-optic-bundle-based optical coherence tomography *Opt. Lett.* **30** 14 1803-5

[5] Kang J U, Han J-H, Liu X, and Zhang K 2010 Common-path optical coherence tomography for biomedical imaging and sensing *J. Opt. Soc. Korea* **14** 1 1-13

[6] Sivak M V Jr, Kobayashi K, Izatt J A, Andrew M, Rollins R, Ung-runyawee R, Chak A, Wong R C K, Isenberg G A and Willis J 2000 High-resolution endoscopic imaging of the gastrointestinal tract using optical coherence tomography *Gastrointest. Endosc.* **51** 474–9

[7] Armstrong J J, Leigh M S, Walton I D, Zvyagin A V, Alexandrov S A, Schwer S, Sampson D D, Hillman D R and Eastwood P R 2003 In vivo size and shape measurement of large hollow organs using endoscopic long-range optical coherence tomography *Opt. Express* **11** 15 1817-26

[8] Xu Y, Singh J, Premachandran 2008 C S, Khairyanto A, Chen K W S, Chen N, Sheppard C J R and Olivo M, Design and development of a 3D scanning MEMS OCT probe using a novel SiOB package assembly *J. Micromech. Microeng.* **18** 125005

[9] Southwell D, Vandegriend B and Basu A 1996 A conical mirror pipeline inspection system *Proc. IEEE Internat. Conf. on Robotics and Automation (22–28 April 1996)* vol 4 pp 3253–8

[10] Suterio R, Goncalves A A Jr. and Cavaco M A 2003 Preliminary evaluation: the indentation method combined with a radial interferometer for residual stress measurement *Proc. SEM Annual Conference & Exposition on Experimental and Applied Mechanics (Charlotte, NC, USA, 2-4 June 2003)*

[11] Isago R and Nakamura K 2009 High-speed imaging with endoscopic optical coherence tomography using bending vibration of optical fiber *20th International Conference on Optical Fibre Sensors: Proc. SPIE 7503, (Edinburgh, UK, 5-9 October 2009)* 75034Y

[12] Hariri L P, Bouma B E, Waxman S, Shishkov M, Vakoc B J, Suter M J, Freilich M I, Oh W-Y, Rosenberg M and Tearney G J 2010 An automatic image processing algorithm for initiating and terminating intracoronary OFDI pullback *Biomed. Opt. Express* **1** 2 566-7